SUPPLEMENTARY MATERIALS

Expanding the amyloid landscape: structural plasticity of antimicrobial peptides

Peleg Ragonis-Bachar[#], Fabio Strati[#], Emil Gustavsson[#], Alexander Khokhlov, Bader Rayan, Eilon Barnea, Alexander Upcher, and Meytal Landau

[#] Equal contribution

Supplementary Tables and Figures:

Supplementary Tables S1-S5

Supplementary Figures S1-S10

Table S1. Database statistics, bioinformatic scheme thresholds and numerical results of prediction

SwissProt Keyword	Antimicrobial	Amphibian defence peptide	antiviral defence	antiviral protein	pathogenic related proteins	prion	virulence	toxin
SwissProt keyword code	KW-0929	KW-0878	KW-0051	KW-0930	KW-0568	KW-0640	KW-0843	KW-0800
Number of peptides	53777	1685	111241	1506	11010	2494	151778	90613
Minimal length	35							
Number of short peptides	897	623	74	21	44	24	101	1383
Prediction of α-helical FF peptides								
Secondary structure was predicted by Jpred[37]								
Minimal length of consecutive residues predicted to have the same SS	5							
Minimal gap length between residues predicted to have a SS	3							
Minimal α-helix average score	7							
Number of peptides passing secondary structure thresholds using Jpred	631	467	31	8	32	21	81	343
Minimal μH (α-helix amphipathicity)	0.46	0.45	0.45	0.5	0.5	0.17	0.63	0.48
Number of peptides passing the μH threshold (predicted as α-helical FF peptides)	314	230	15	4	16	5	60	179
Prediction of SSW FF peptides								
Secondary structure was predicted by Tango[1]								

Minimal length of consecutive residues predicted to have the same SS	5							
Minimal gap length between residues predicted to have a SS	3							
Number of peptides passing minimal consecutive residues and gap length thresholds	440	262	43	6	18	9	48	591
Maximal difference between α-helix and beta SS propensity scores	1.67	1.26	2.52	2.2	1.72	2.3	3.34	2.4
Minimal hydrophobicity (H)	0.46	0.5	0.51	0.56	0.52	0.7	0.49	0.42
Number of peptides passing the H threshold (predicted as SSW FF peptides)	181	90	22	3	8	5	31	313
Number of peptides predicted to be both α-helical and SSW FF-peptides	96	46	1	1	5	0	30	67
Number of peptides with antimicrobial annotation	897	400	4	9	0	0	0	92
Number of antimicrobial peptides predicted as both α-helical and SSW FF-peptides	96	36	0	1	0	0	0	20

For each functional group, defined by SwissProt keywords, the total number of proteins and the number of peptides shorter than 35 residues are indicated. Two computational routes for predicting fibril-forming (FF) peptides are shown: α-helical and α/β secondary structure-switching (SSW) pathways. For each route, the method used to calculate secondary structures (SS), the applied threshold values, and the number of peptides passing these thresholds are specified. Thresholds were either fixed (general cutoffs) or based on the average value calculated within each keyword-defined group. Finally, the number of short peptides in each group annotated (also) as antimicrobial is provided, along with the subset predicted as both α-helical and SSW FF-peptides. In total, 835 unique sequences were identified as α-helical or α/β secondary structure-switching fibril-forming peptides.

Table S2. **Source organisms and sequences of the experimentally tested peptides**

Title	Source organism	Sequence
Brevinin-1OKc	Nidirana okinavana (Kampira Falls frog) (Babina okinavana)	FFGSIIGALAKGLPSLISLIKK-NH2
Osmin	Osmia rufa (Red mason bee)	GFLSALKKYLPIVLKHV-NH2
Chrysophsin-3	Pagrus major (Red sea bream) (Chrysophrys major)	FIGLLISAGKAIHDLIRRRH-NH2
Melectin	Melectaalbifrons (Cuckoo bee) (Melecta punctata)	GFLSILKKVLPKVMAHMK-NH2
Phylloseptin-2.1TR	Phyllomedusa trinitatis (Trinidad leaf frog)	FLSLIPHIATGIAALAKHL-NH2
Polybia-CP	Polybia paulista (Neotropical social wasp) (Swarm-founding polistine wasp)	ILGTILGLLKSL-NH2
Grammistin Pp 2a	Pogonoperca punctata (Clown grouper) (Grammistes punctatus)	FIGGIISLIKKLF
Panurgin 1	Panurgus calcaratus (Solitary bee)	LNWGAILKHIIK-NH2
Temporin-1ITa	Rana italica (Italian stream frog) (Rana graeca italica)	FLGAIAQALTSLLGKL-NH2
Hemolysin H2U	Staphylococcus cohnii subsp. urealyticus	MDFIIDIIKKIVGLFTGK
Dahlein-5.6	Ranoidea dahlii (Dahl's aquatic frog) (Litoria dahlii)	GLLASLGKVFGGYLAEKLKPK
Eumenitin	Eumenes rubronotatus (Solitary wasp)	LNLKGIFKKVASLLT
Decoralin	Oreumenes decoratus (Potter wasp)	SLLSLIRKLIT
Vespid chemotactic peptide 5e (Vespid-CP 5e)	Vespa magnifica (Hornet)	FLPIIAKLLGGLL
Riparin-2.1	Crinia riparia (Streambank froglet) (Flinders Ranges froglet)	IIEKLVNTALGLLSGL-NH2
Protonectin (Agelaia-chemotactic peptide - Agelaia-CP)	Agelaia pallipes pallipes (Neotropical social wasp)	ILGTILGLLKGL
Aurein 1.2	Ranoidea raniformis (Southern bell frog) (Litoria raniformis)	GLFDIIKKIAESF-NH2

Table S3. **Database annotations of the experimentally tested peptides**

Title	Uniprot	Uniprot Homologs	Uniprot Keyword	PDB	Pubmed	GO
Brevinin-1OKc	C0HL10		Antimicrobial		15629529	GO:0005576 GO:0031640 GO:0050829 GO:0050830
Osmin	P0CD70		Antimicrobial		19109988	GO:0005576 GO:0042742 GO:0044179 GO:0050832 GO:0090729
Chrysophsin-3	P83547		Antimicrobial		12581207	GO:0005576 GO:0006952 GO:0044179 GO:0050829 GO:0050830
Melectin	P86170		Antimicrobial		18942691	GO:0005576 GO:0035895 GO:0044179 GO:0050829 GO:0050830 GO:1990142
Phylloseptin-2.1TR	C0HLD7	P84930	Amphibian defense peptide, Antimicrobial		29980138; 30734396	GO:0005576 GO:0042742 GO:0044179 GO:0045087 GO:0050832
Polybia-CP	P0C1R0		Antimicrobial		16129513; 21745529; 22450985; 23836163; 30534613; 32360153	GO:0005576 GO:0006935 GO:0016020 GO:0050829 GO:0050830 GO:0050921
Grammistin Pp 2a	P69843		Antimicrobial		15777955	GO:0005576 GO:0042742 GO:0044179
Panurgin 1	C0HL84		Antimicrobial		23483218	GO:0005576 GO:0016020 GO:0031640 GO:0044179 GO:0050829 GO:0050830 GO:0050832 GO:0051673 GO:0051715
Temporin-1ITa	C0HL49		Amphibian defense peptide, Antimicrobial		28699258	GO:0005576 GO:0042742 GO:0044179 GO:0050832

Hemolysin H2U	P85223	P85220	Virulence		18752624	GO:0005576 GO:0044179 GO:0090729
Dahlein-5.6	P84272		Amphibian defense peptide		11555873	GO:0005576 GO:0006952 GO:0030235 GO:0051001
Eumenitin	P0C931		Antimicrobial		11006592; 16762455; 18206199	GO:0005576 GO:0006811 GO:0016021 GO:0042742 GO:0043303
Decoralin	P85870		Antimicrobial	2N9A	17981364; 27096870; 28267894	GO:0005576 GO:0016020 GO:0019835 GO:0031640 GO:0042832 GO:0043303 GO:0043306 GO:0050829 GO:0050830 GO:0050832
Vespid-CP 5e	P0C1M1		Antimicrobial		16330062	GO:0005576 GO:0042742 GO:0043303 GO:0044179 GO:0050832
Riparin-2.1	P86127		Amphibian defense peptide, Antimicrobial		16470724; 18601958	GO:0005576 GO:0050830
Agelaia-CP	P69437	P0C1R1	Antimicrobial	6N68, 7JGY	15052574; 15225564; 23836163	GO:0005576 GO:0006935 GO:0016020 GO:0042742
Aurein 1.2	P82387		Amphibian defense peptide, Antimicrobial	1VM5	10951191	GO:0005576 GO:0042742

Table S4. Biochemical properties and secondary structure prediction of the experimentally tested peptides

Protein names	Length	Charge	Hydrophobicity (full length)	uH (full length)	uH (helical part)	SS score difference	FF-peptide prediction
Brevinin-1OKc	22	3	0.72	0.58	0.61	0.23	α-helix + SSW
Osmin	17	3	0.70	0.53	0.51	1.31	α-helix + SSW
Chrysophsin-3	20	3	0.51	0.47	0.74	0.85	α-helix + SSW
Melectin	18	4	0.60	0.52	0.55	1.14	α-helix + SSW
Phylloseptin-2.1TR	19	1	0.81	0.53	0.50	0.50	α-helix + SSW
Polybia-CP	12	1	0.94	0.68	0.63	1.60	α-helix + SSW
Grammistin Pp 2a	13	2	0.94	0.75	0.75	1.44	α-helix + SSW
Panurgin 1	12	2	0.74	0.54	0.79	1.50	α-helix
Temporin-1ITa	16	1	0.75	0.60	0.60	0.13	α-helix + SSW
Hemolysin H2U	18	1	0.69	0.55	0.65	1.52	α-helix + SSW
Dahlein-5.6	21	3	0.44	0.34	0.62	0.46	α-helix + SSW
Eumenitin	15	3	0.57	0.46	0.67	0.78	α-helix + SSW
Decoralin	11	2	0.78	0.65	0.71	0.19	α-helix + SSW
Vespid-CP 5e	13	1	1.07	0.61	0.56	0.43	α-helix + SSW
Riparin-2.1	16	0	0.73	0.58	0.60	1.18	α-helix + SSW
Agelaia-CP	12	1	0.95	0.68	0.63	1.02	α-helix + SSW
Aurein-1.2	13	0	0.58	0.77	0.83	0.45	α-helix + SSW

Biochemical properties of the selected peptides, including peptide length, net charge at pH 7.4, overall hydrophobicity (H), and hydrophobic moment (μH) calculated for both the full-length sequence and the predicted α-helical segment. The table also includes the average score difference between α-helix and β-sheet predictions based on Tango[1] analysis, and the predicted classification of each peptide as a fibril-forming peptide (ff-peptide) with either α-helical or secondary structure-switching (SSW) propensity.

Table S5. Cryo-EM data collection, refinement and validation statistics

	Aurein 1.2		**Brevinin-1OKc**			
	ddH2O Pol I	ddH2O Pol II	ddH2O Pol I	ddH2O Pol II	PBS pH6.5 Pol I	PBS pH6.5 Pol II
Magnification	105000		105000		105000	
Voltage (kV)	300		300		300	
Electron Exposure	40		50		50	
Defocus range	-0.5,-1,-1.5,-2,-2.5,-3,-3.5		-0.5 to -2		-0.5 to -2	
Pixel size	0.85		0.85		0.825	
Nr. of micrographs	13396		10018		6236	
Nr. of initial particles	1418345	131027	1569255	443921	1523940	328282
Nr. of particles for reconstruction	185612	90810	349067		498395	312286
Symmetry imposed	C2	C1	C1	C2	C2	C2
Cross-over (Å)						
Twist (°)	-1.18	-2.40	-180.76		59.49	59.5
Rise (Å)	4.84	4.84	2.39		1.6	1.6
Map resolution (Å)	2.80	3.78	3.31		2.17	2.28
Map B-factor(Å²)	-71	-110	-91		-36	-34
Molprobity	1.49	1.94	1.45		0.86	1.06

score						
Clashscore	1.72	2.29	8.20		1.34	2.71
Rama Plot						
Favoured	97.73	90.15	100		100	99.17
Allowed	2.27	9.85	0		0	0.83
Outlier	0	0	0		0	0

This table provides the parameters and statistics for the data collection, processing, refinement, and structure validation of the cryo-EM structures. Refinement statistics were generated using either the Phenix or Servalcat package [2,3].

Figure S1. **Thioflavin-T fibrillation kinetics assay**

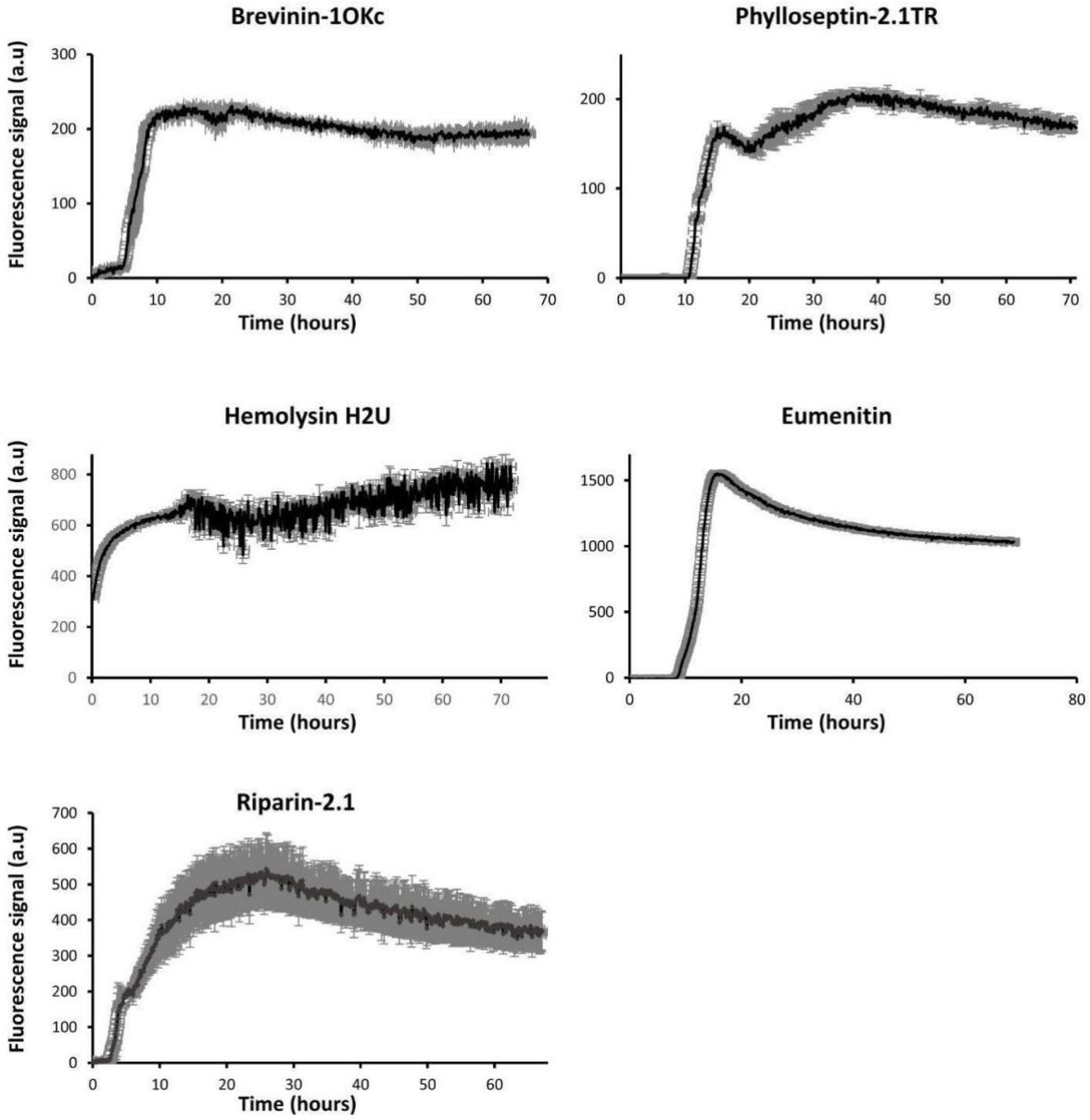

Fibrillation kinetics assays were performed using 100 μM peptide and 200 μM ThT in a potassium phosphate buffer at pH 7.4. The graph shows mean fluorescence readings of triplicate measurements of the peptides over a period of 70-80 hours. Error bars represent the standard error of the mean. The peptides display a characteristic fibrillation curve, following a lag time varying from 1-10 hours. The peptides not mentioned here failed to produce any fluorescence signal above negative control levels.

Figure S2. Secondary structure analysis of the peptides in the solid state using Attenuated total internal reflection (ATR) Fourier transform infrared (FTIR) spectroscopy

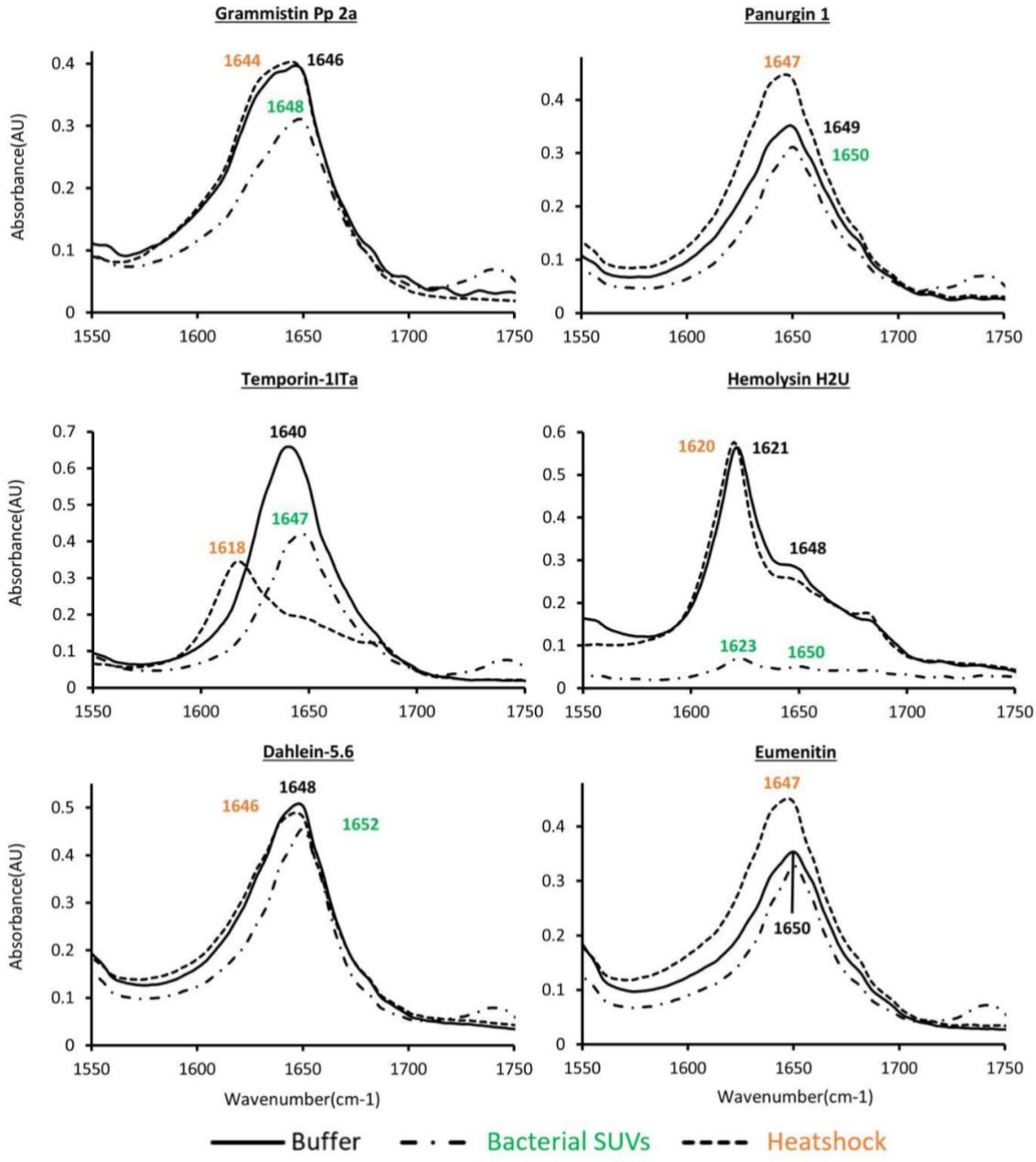

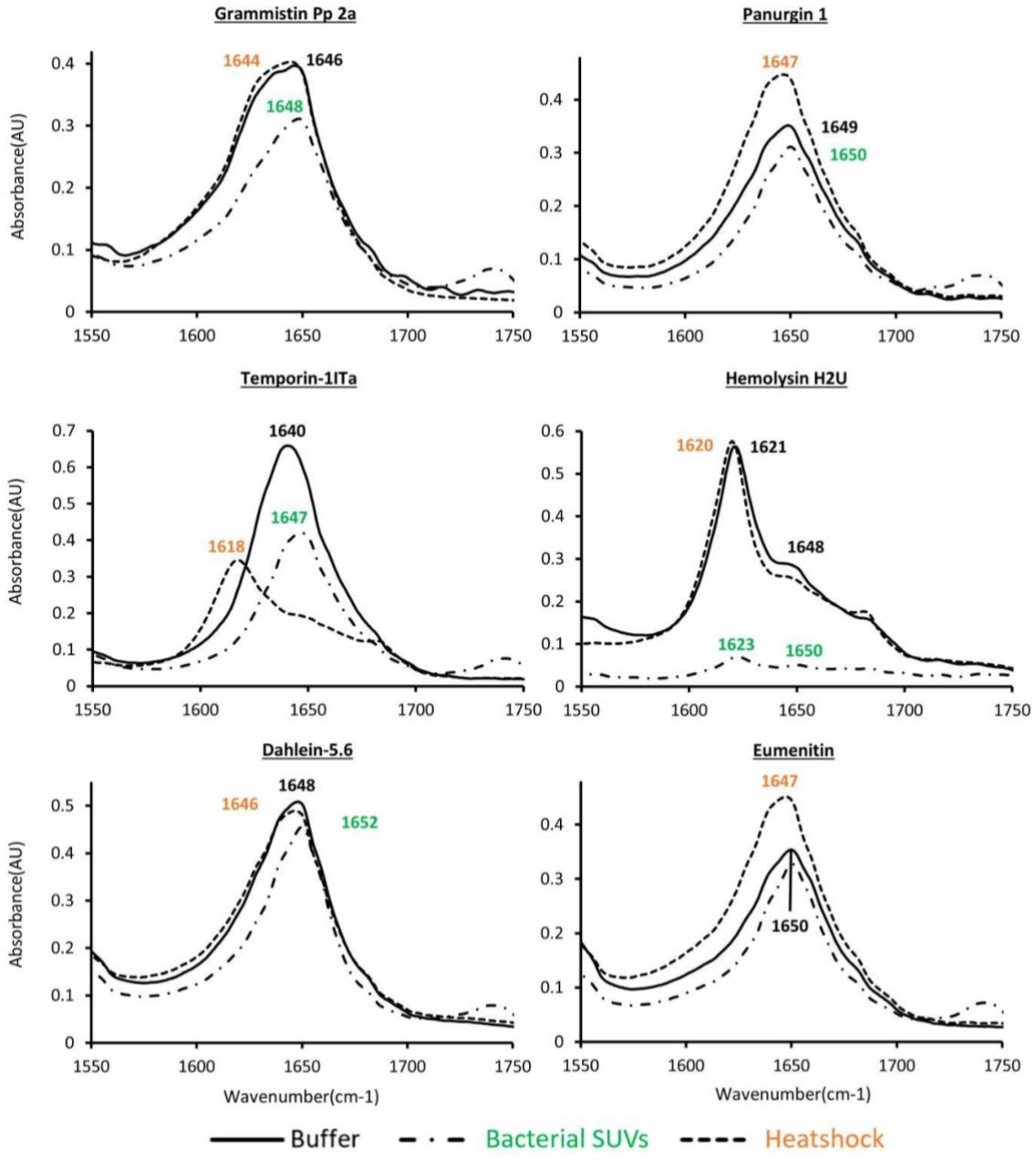
Grammistin Pp 2a
1644
1646
1648
Panurgin 1
1647
1649
1650
Temporin-1ITa
1640
1647
1618
Hemolysin H2U
1620
1621
1648
1623
1650
Dahlein-5.6
1648
1646
1652
Eumenitin
1647
1650
Absorbance(AU)
Wavenumber(cm-1)
Buffer
Bacterial SUVs
Heatshock

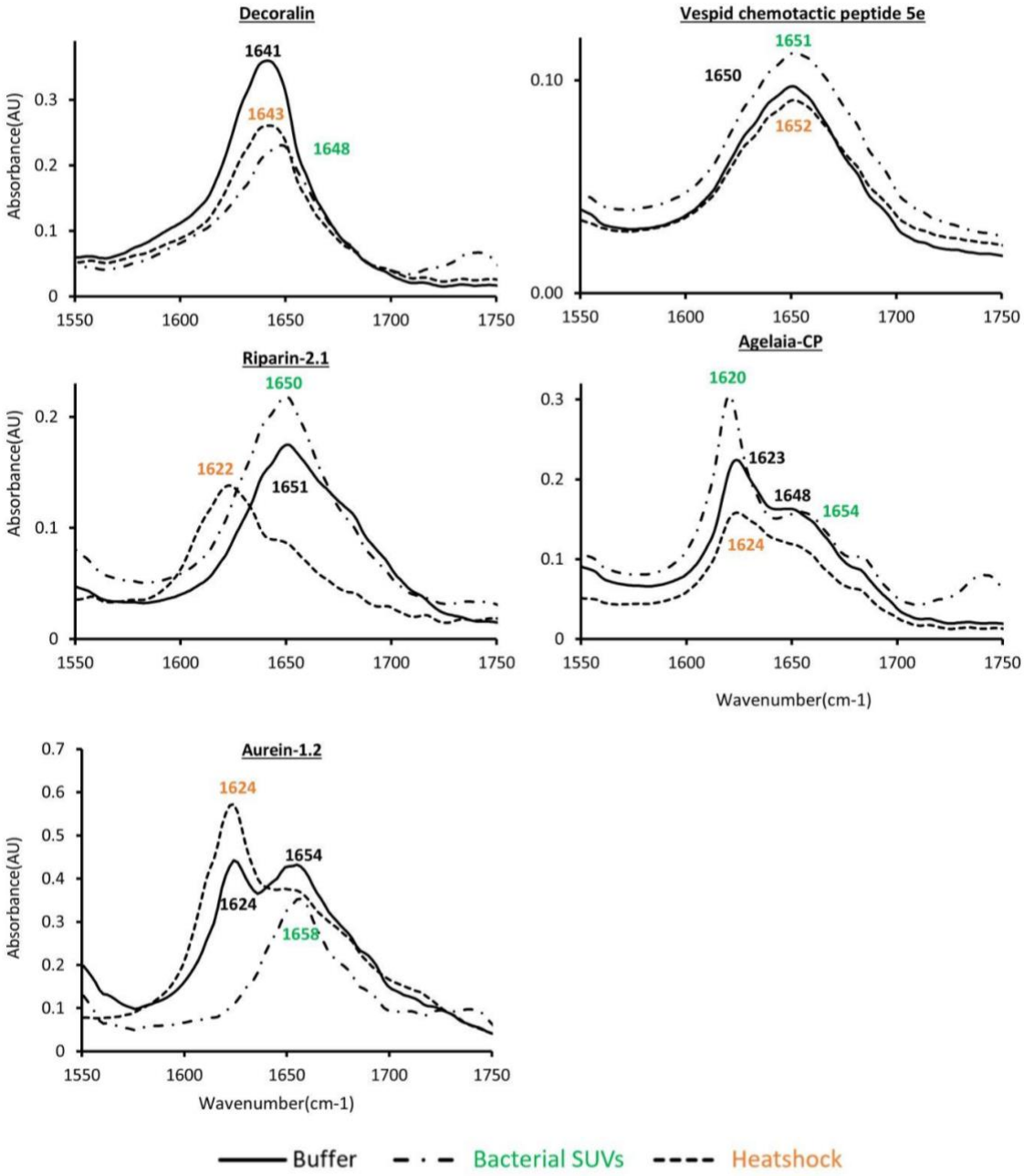

Spectra of the amide I′ region under various conditions. All peptides were incubated for 2 hours in a 10 mM sodium phosphate buffer at pH 7.5. Solid curve: spectra of peptides solely in buffer. Dashed curve: peptides incubated in buffer in the presence of liposomes composed of 1:1 DOPE: DOPG, mimicking a Gram-positive bacterial membrane. Dotted curve: spectra are of the peptides incubated in the buffer for 2 hours and then subjected to a heat shock at 80°C for 10 minutes. The peaks are described by number and colored by condition: buffer (black), presence of liposome's (green), and after heat shock (orange). The peaks were determined based on the calculated second derivative provided by the OMNIC software. The equipment and software services were provided by the Laboratory for Physical Measurements, managed by Dr. Inna Zeltser from the Department of Materials Science and Engineering at the Technion - Israel Institute of Technology.

Figure S3. Cryo-EM representative micrographs and 2D class averages of aurein 1.2

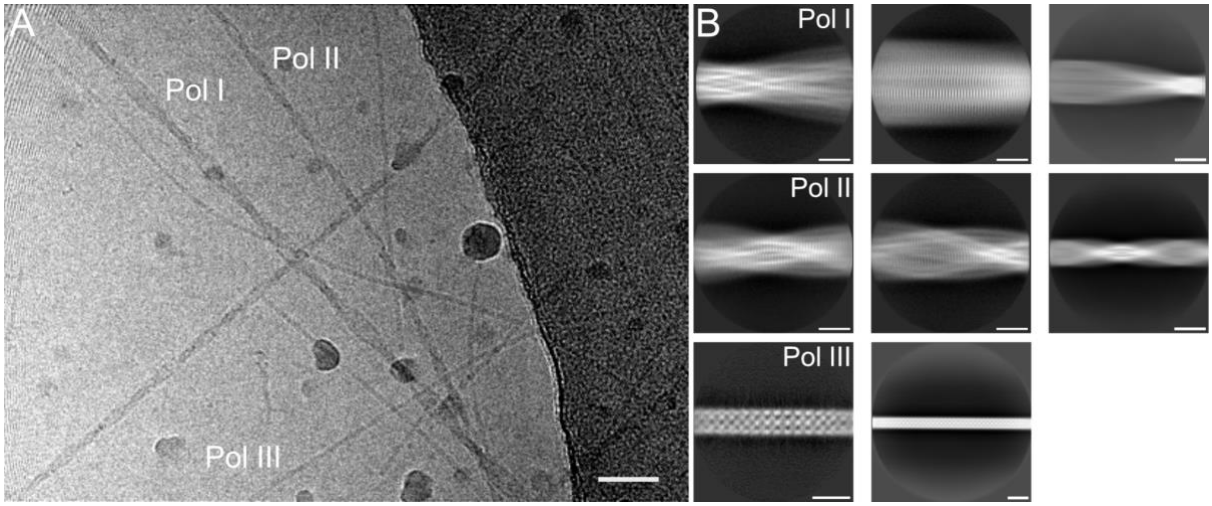

Three main fibril polymorphs of aurein 1.2 were observed in ddH_2O. Polymorphs I and II displayed well-defined twists, clearly visible in the micrographs (**A**) and corresponding 2D class averages (**B**). In addition, a third fibril type was detected which, in both micrographs and 2D classes, lacked any discernible twist and exhibited a 'checkerboard-like' arrangement, suggesting that it may not behave as a canonical amyloid fibril.

Figure S4. Cryo-EM map and model overviews of aurein 1.2 polymorph I

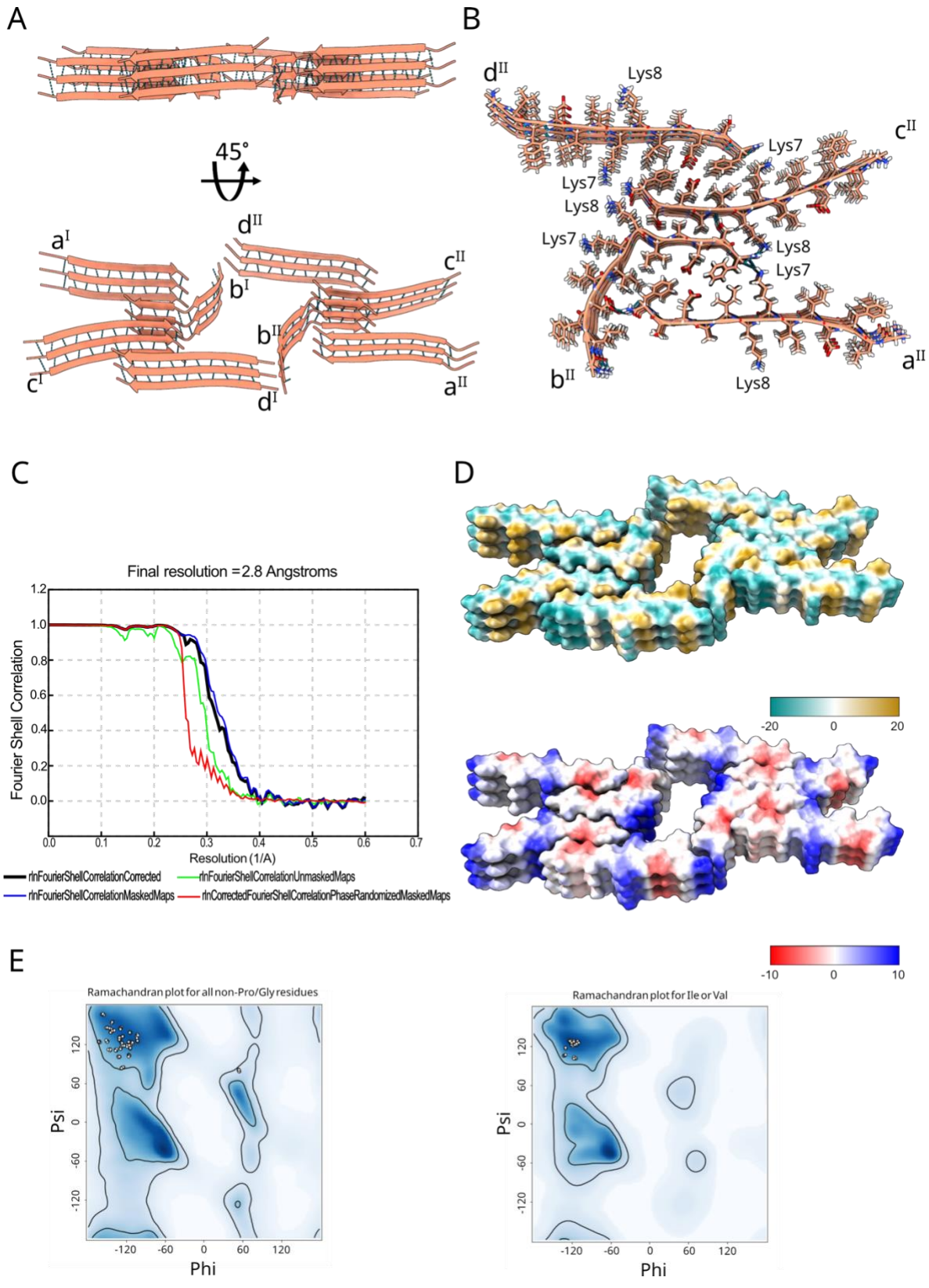

(**A**) Top and side views of the Polymorph I model highlighting hydrogen bond formation between the β-sheet layers. (**B**) Top-tilted view of one of the protofilaments showing side chains and illustrating the steric zipper interface. The conserved lysine residues are specifically indicated. (**C**) Gold-standard Fourier shell correlation (GSFSC) curve reported by Relion for the Polymorph I map. (**D**) Surface representations of Polymorph I are colored by calculated hydrophobic (top) and electrostatic (bottom) properties; scale bar included. (**E**) Ramachandran plot[4] of the final model, showing that most residues fall within the β-sheet range (top left) and one residue at the edge of the left handed α-helix basin (top-middle right) consistent with the observed kink in the backbone conformation.

Figure S5. Cryo-EM map and model overviews of aurein 1.2 polymorph II

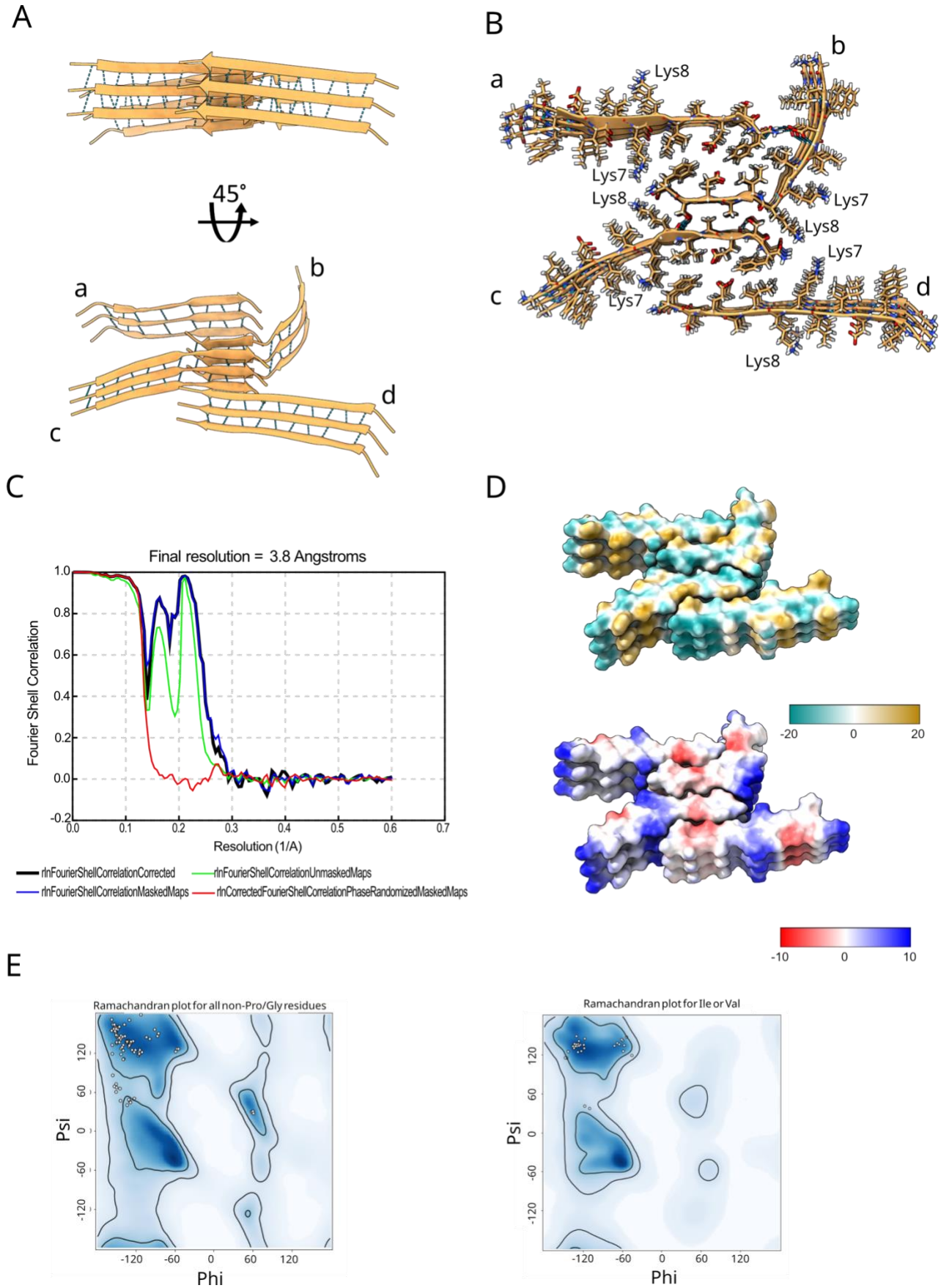

(**A**) Top and side views of the Polymorph II model highlighting hydrogen bond formation between the β-sheet layers. (**B**) Top-tilted view showing side chains and illustrating the steric zipper interface. The conserved lysine residues are specifically indicated. (**C**) GSFSC curve reported by Relion for the Polymorph II map. Of note, the covalent bond to the C-terminal amidation modification is not seen. (**D**) Surface representations of Polymorph II are colored by calculated hydrophobic (top) and electrostatic (bottom) properties; scale bar included. (**E**) Ramachandran plot[4] of the final model, showing that most residues fall within the β-sheet range (top left), with one residue located at the edge of the left-handed α-helix basin (upper-middle right) and an additional cluster situated between the canonical β-sheet and α-helical basins (left). This distribution likely reflects the kink within the β-sheets and the presence of extended or turn-like conformations, indicating deviations from a fully canonical β-sheet architecture, although the data can also be affected by the relatively low resolution of this polymorphs map (3.80 Å).

.

Figure S6. Cryo-EM representative micrographs and 2D class averages of brevinin-1OKc fibrils under different incubation conditions

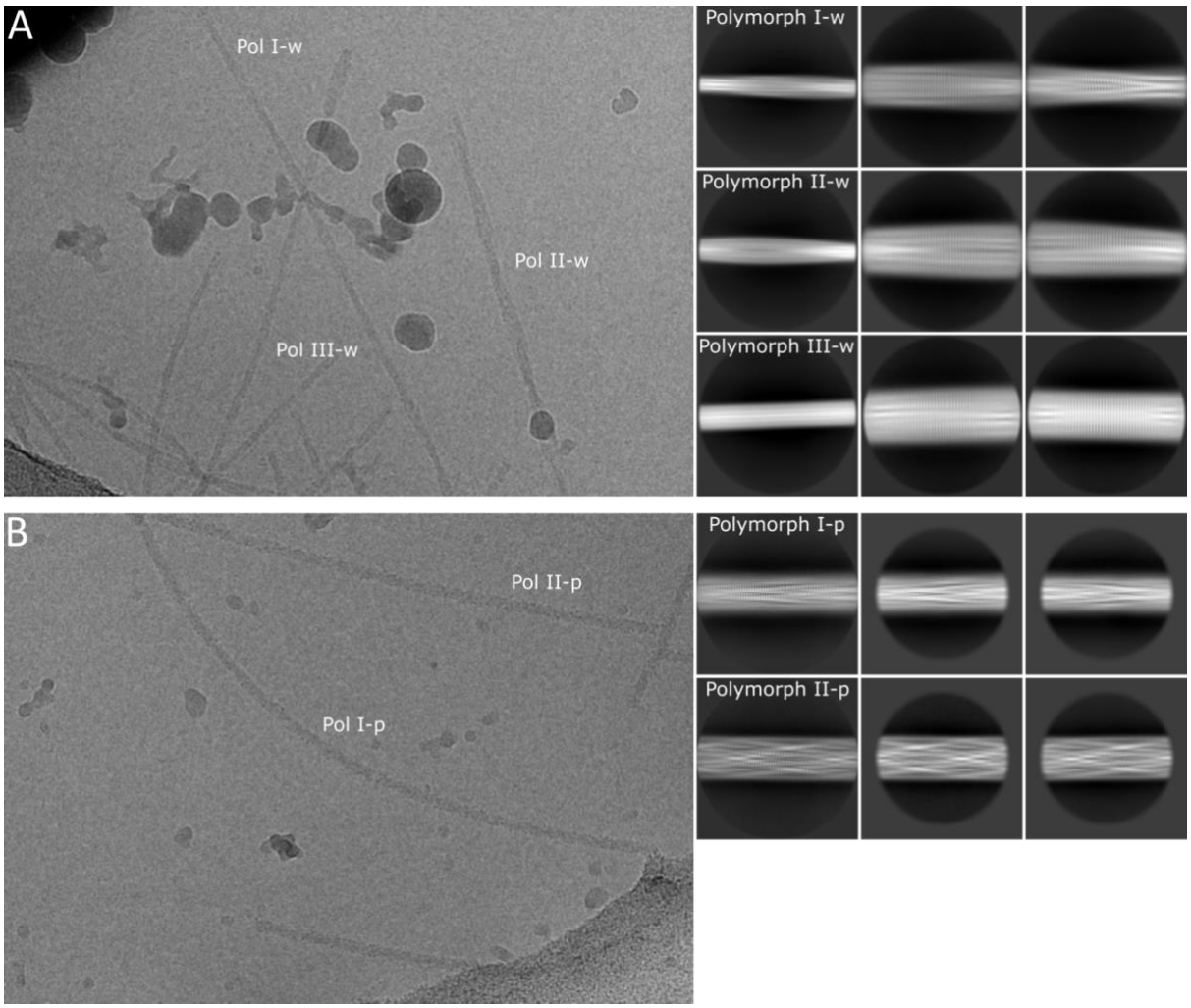

(**A**) Three fibril polymorphs were identified for brevinin-1OKc incubated in ddH_2O. Polymorph I-w displays a well-defined screw-symmetric architecture with two peptide chains forming the ordered fibril core. Polymorph II-w also consists of two protofilaments arranged similarly to I-w. In contrast, Polymorph III-w shows no detectable helical twist, precluding high-resolution reconstruction by standard helical methods. (**B**) Two fibril polymorphs were observed for brevinin-1OKc incubated in 10 mM PBS at pH 6.5, designated I-p and II-p. These fibrils exhibit more complex amyloid architectures compared to those grown in ddH_2O, yet remain consistent with a cross-β arrangement, as indicated by the characteristic ~4.75 Å layer line spacing and the pattern of hydrogen bonds (Figure S7-S9).

Figure S7. Cryo-EM map and model overviews of brevinin-1OKc Polymorph I-w

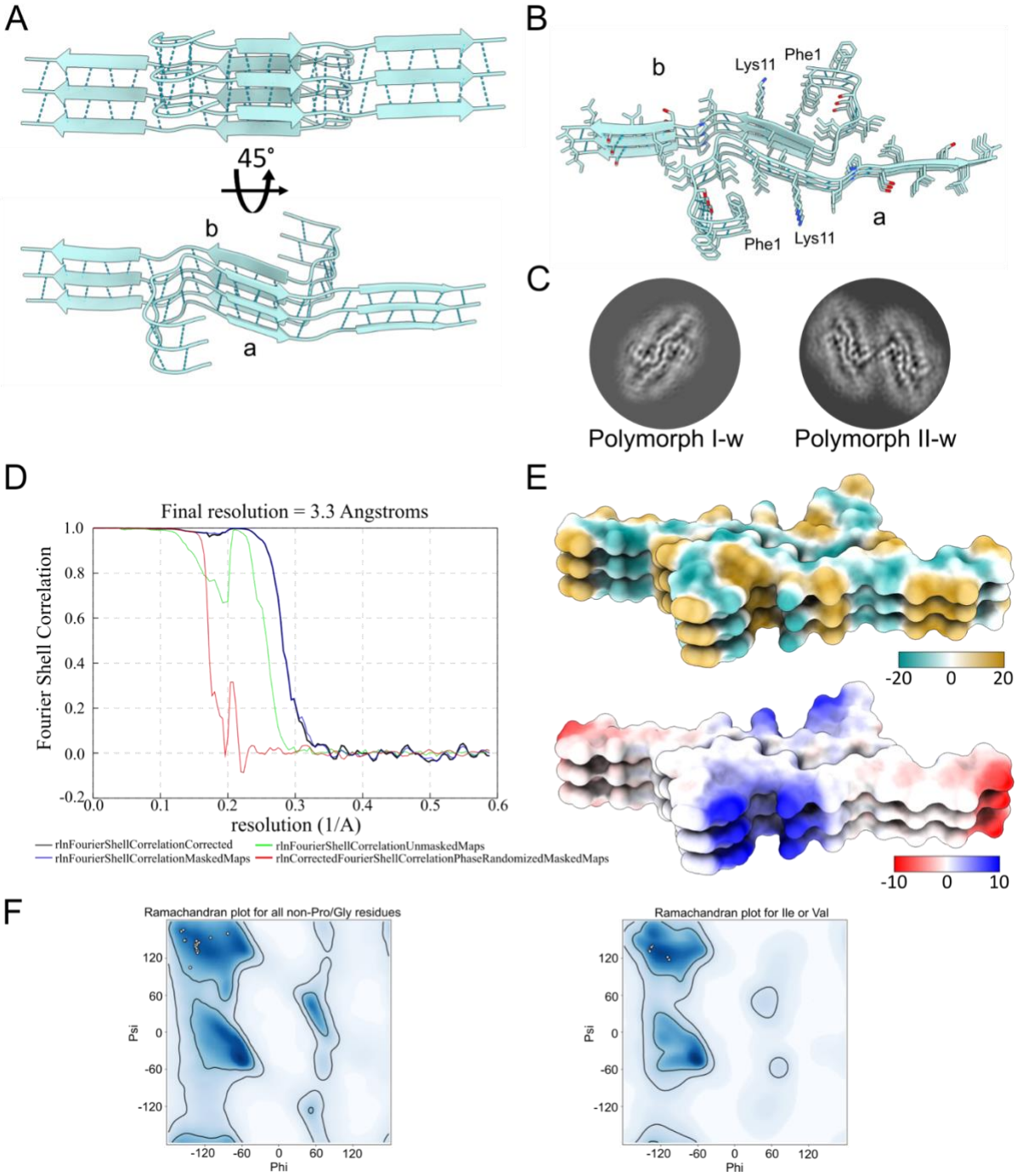

(**A**) Top and side views of the Polymorph I-w atomic model highlighting hydrogen bond formation between the β-sheet layers. (**B**) Top-tilted view showing side chains and illustrating the steric zipper interface. (**C**) Structural comparison of Polymorphs I-w and II-w. (**D**) GSFSC curve reported by Relion for the Polymorph I-w map. (**E**) Surface representations of Polymorph I-w are colored by calculated hydrophobic (top) and electrostatic (bottom) properties; scale bar included. (**F**) Ramachandran plot[4] of the final model, showing that most residues fall within the β-sheet region (top left). In this polymorph, the kink is introduced by a glycine residue, which does not appear as a deviation in the Ramachandran plot due to its broader conformational flexibility.

Figure S8. Cryo-EM map and model overviews of brevinin-1OKc Polymorph I-p

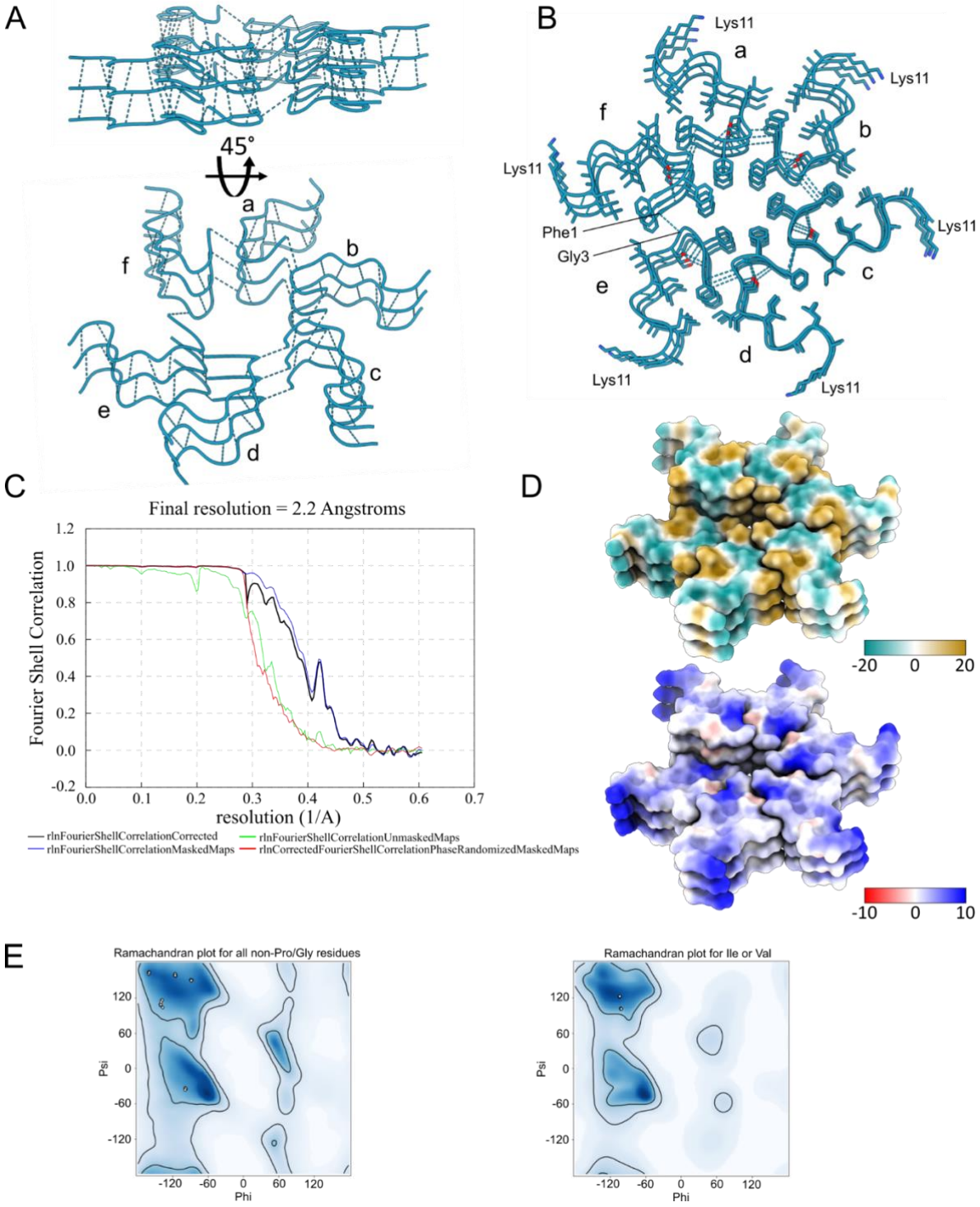

(**A**) Top and side views of the Polymorph I-p atomic model highlighting hydrogen bond formation between the β-sheet layers and between β-sheets. (**B**) Top-tilted view showing side chains and illustrating the steric zipper interface. (**C**) GSFSC curve reported by Relion for the Polymorph I-p map. (**D**) Surface representations of Polymorph I-p are colored by calculated hydrophobic (top) and electrostatic (bottom) properties; scale bar included. (**E**) Ramachandran plot[4] of the final model, showing that most residues fall within the β-sheet range (top left), with one residue positioned within a region indicating a right-handed or a tighter α-helix (lower-middle left), likely reflecting the kink.

Figure S9. Cryo-EM map and model overviews of brevinin-1OKc Polymorph II-p

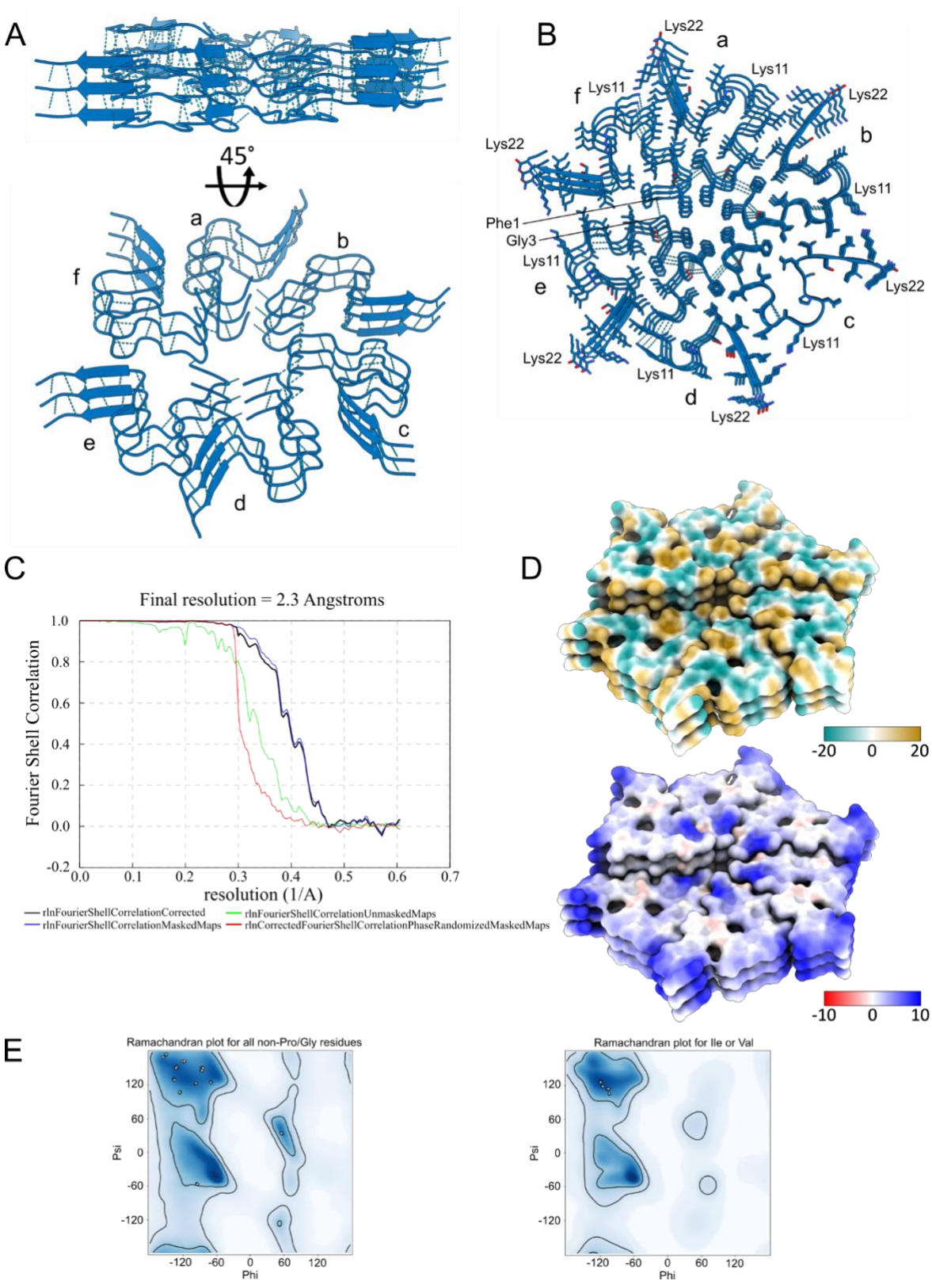

(**A**) Top and side views of the Polymorph II-p atomic model highlighting hydrogen bond formation between the β-sheet layers and between β-sheets. (**B**) Top-tilted view showing side chains and illustrating the steric zipper interface. (**C**) GSFSC curve reported by Relion for the Polymorph II-p map. (**D**) Surface representations of Polymorph II-p are colored by calculated hydrophobic (top) and electrostatic (bottom) properties; scale bar included. (**E**) Ramachandran plot[4] of the final model, showing that most residues fall within the β-sheet range (top left), with one residue located near the boundary of the α-helical basin (middle–lower left), consistent with a right-handed α-helix, a tighter 3_{10}-helix, or a turn-like conformation, while another residue falls within the left-handed α-helix region (upper right). This distribution likely reflects the kink within the β-sheets and the presence of extended or turn-like conformations, indicating deviations from a fully canonical β-sheet architecture.

Figure S10. Sequence comparison of amphibian AMPs

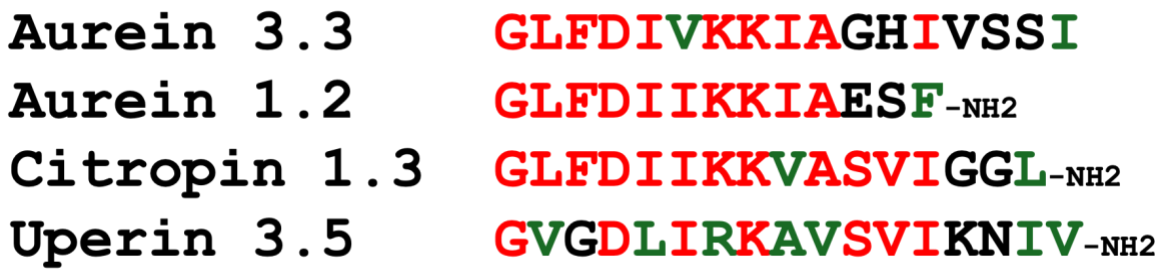

Sequences of several amyloid-forming AMPs from the aurein, citropin and uperin families with known structures[5–7] are shown. Residues identical in at least two peptides are highlighted in red, while positions with residues sharing similar biophysical properties are marked in green.

References

1. Rousseau, F., Schymkowitz, J. & Serrano, L. Protein aggregation and amyloidosis: confusion of the kinds? *Curr. Opin. Struct. Biol.* **16**, 118–126 (2006).
2. Liebschner, D. *et al.* Macromolecular structure determination using X-rays, neutrons and electrons: recent developments in Phenix. *Acta Crystallogr. D Struct. Biol.* **75**, 861–877 (2019).
3. Yamashita, K., Palmer, C. M., Burnley, T. & Murshudov, G. N. Cryo-EM single-particle structure refinement and map calculation using Servalcat. *Acta Crystallogr. D Struct. Biol.* **77**, 1282–1291 (2021).
4. Ramachandran, G. N., Ramakrishnan, C. & Sasisekharan, V. Stereochemistry of polypeptide chain configurations. *J. Mol. Biol.* **7**, 95–99 (1963).
5. Strati, F. *et al.* Structural and functional versatility of the amyloidogenic non-amidated variant of the antimicrobial peptide citropin 1.3. *Adv. Sci. (Weinh.)* e03997 (2025) doi:10.1002/advs.202503997.
6. Bücker, R. *et al.* The Cryo-EM structures of two amphibian antimicrobial cross-β amyloid fibrils. *Nat. Commun.* **13**, 4356 (2022).
7. Salinas, N. *et al.* The amphibian antimicrobial peptide uperin 3.5 is a cross-α/cross-β chameleon functional amyloid. *Proceedings of the National Academy of Sciences* **118**, (2021).